IBRACON Structures and Materials Journal
Revista IBRACON de Estruturas e Materiais
ISSN 1983-4195 ismj.org

ORIGINAL ARTICLE

Punching shear design with control perimeters subjected to asymmetrical bending

Verificação à punção com perímetros de controle submetidos à flexão assimétrica

Mariana Nunes Souza[a]
Mayra Soares Pereira Lima Perlingeiro[a]
Mauro Schulz[a]

[a]Universidade Federal Fluminense – UFF, Civil Engineering Department, Niteroi, RJ, Brasil

Received 19 September 2022
Accepted 23 March 2023

Abstract: A numerical procedure is proposed for asymmetrical plastic shear diagrams in punching control perimeters. Asymmetrical diagrams occur for edge and corner columns and for internal columns with biaxial unbalanced moments. The procedure intends to support the use of NBR 6118, which covers asymmetrical shear distributions due to internal moments of edge and corner columns. The study of columns in different positions of the slab proves the robustness and numerical efficiency of the proposal. The practical application of the procedure is tested against Model Code 1990, Eurocode 2, NBR 6118, and with combinations of criteria from these codes. The estimated capacities are compared with experimental data from the literature. Eurocode 2 initially presents better results, but this code does not consider moments with internal eccentricities in edge and corner columns. The Eurocode 2 evaluations are significantly improved by the inclusion of NBR 6118 criteria that partially apply these moments, whose asymmetrical shear diagrams can be determined by the proposed procedure.

Keywords: flat slabs, punching shear, unbalanced moments, plastic analysis.

Resumo: Um procedimento numérico é proposto para diagramas plásticos de cisalhamento assimétricos em perímetros de controle de punção. Diagramas assimétricos ocorrem para pilares de borda e de canto e para pilares internos com momentos desbalanceados biaxiais. O procedimento visa auxiliar a utilização da NBR 6118, que considera as distribuições assimétricas de cisalhamento associadas aos momentos internos de pilares de borda e de canto. O estudo de pilares em diferentes posições da laje comprova a robustez e a eficiência numérica da proposta. A aplicação prática do procedimento é testada com o Model Code 1990, o Eurocode 2, a NBR 6118 e com combinações de critérios desses códigos. As capacidades estimadas são comparadas com dados experimentais da literatura. O Eurocode 2 apresenta inicialmente melhores resultados, mas este código não considera os momentos com excentricidades internas em pilares de borda e de canto. As estimativas do Eurocode 2 são significativamente melhoradas pela inclusão de critérios da NBR 6118 que aplicam parcialmente esses momentos, cujos diagramas de cisalhamento assimétricos podem ser determinados pelo procedimento proposto.

Palavras-chave: lajes lisas, punção, momentos desbalanceados, análise plástica.

How to cite: M. N. Souza, M. S. P. L. Perlingeiro, and M. Schulz, "Punching shear design with control perimeters subjected to asymmetrical bending," *Rev. IBRACON Estrut. Mater. J.*, vol. 16, no. 3, e16307, 2023, https://doi.org/10.1590/S1983-41952023000300007

1 INTRODUCTION

The design of flat slabs is often controlled by the punching shear strength of the slab-column connections. Slab-column connections are usually subjected to unbalanced moments that yield additional shear stresses and reduce the punching shear capacity.

Corresponding author: Mauro Schulz. E-mail: mschulz@id.uff.br
Financial support: None.
Conflict of interest: Nothing to declare.
Data Availability: Data-sharing is not applicable to this article as no new data were created in this study.

Eurocode 2 [1] and the Brazilian code NBR 6118 [2] adopt the Model Code 90 [3] punching shear design model with modifications. In this work, these codes are referenced by the abbreviations EC2, NBR6118, and MC90, respectively. The MC90 model compares acting stresses with resisting stresses in control perimeters.

Shear forces due to normal forces are assumed to be uniformly distributed along control perimeters or reduced control perimeters. Shear forces distributed due to unbalanced moments are considered fully plastic in both positive and negative directions. The positive and negative parts of the perimeter may show symmetry, but they are often asymmetrical. Plastic asymmetrical bending diagrams require nonlinear solutions.

This paper proposes a numerical procedure for the determination of asymmetrical plastic shear diagrams in arbitrary control perimeters. The procedure is tested together with the empirical equations set forth in MC90, EC2, and NBR6118. The results are compared with experimental data from the literature.

2 SELECTED RECOMMENDATIONS FROM THE CODES

Research that influenced the design of the MC90 model is discussed by Regan [4] and Regan and Braestrup [5]. The ACI 318-19 [6] and Model Code 2010 [7] recommendations are not discussed here. ACI 318-19 adopts the linear elastic hypothesis proposed by di Stasio and van Buren [8]. Model Code 2010 verifies plastic distributions based on the Critical Shear Crack Theory (Muttoni [9] and Ruiz and Muttoni [10]).

MC90, EC2, and NBR6118 verify the capacity of slabs without transverse reinforcement at Perimeter 1. Perimeter 1 is at distance $2d$ from the column face, where d is the effective depth of the slab. Considering elements without shear reinforcement, the punching strength of slabs at Perimeter 1 corresponds to the shear strengths of the linear members (FIB Bulletin 2 [11]). The three codes present equivalent expressions for design shear stresses τ_{Rd}, whose parameters are determined using the respective partial safety factors for concrete γ_c.

Compressive stresses in concrete struts are verified at Perimeter 0, which is adjacent to the column. Although the τ_{Rd} expressions are similar at Perimeter 0, MC90, EC2, and NBR6118 reduce the diagonal compressive capacity by different factors.

Perimeter n is tested when transverse reinforcement is required. The distance between this perimeter and the outer reinforcement contour is kd. MC90 and NBR6118 use $k = 2$, while EC2 uses $k = 1.5$. The three codes define maximum stresses for transverse reinforcement but use different approaches.

The differences between the codes are more significant in the control perimeters submitted to bending. The plastic diagrams of internal columns subjected to biaxial bending are asymmetrical. This issue is only addressed in EC2, which indicates an empirical solution. MC90 and EC2 ignore moments with internal eccentricity in edge and corner columns. NBR6118 partially includes internal moments of edge and corner columns when their eccentricities are greater than the eccentricities between the columns and the reduced control perimeters.

3 PUNCHING SHEAR DESIGN WITH UNBALANCED MOMENTS

Any evaluation of shear forces along a control perimeter must consider that the bending and torsional moments resist part of the unbalanced moment. The K factor is defined as the fraction of the unbalanced moment that is resisted by shear forces.

The moments transferred to the slab by bending and shear are experimentally investigated by Hanson and Hanson [12] on square columns. The ratios of unbalanced moments resisted by shear are analytically discussed by Mast [13] for internal columns (Figure 1). The corresponding K factor is estimated by the elastic solution of a plate subjected to a concentrated moment. The plate is simply supported in the main direction and is infinite in the other direction (Girkmann [14]). The K factor can be defined as a function of the control perimeter shape in the region close to the column.

Design K values indicated in MC90 are compared with Mast's [13] approximate elastic solution (Figure 1). The analytical values assume that lengths a and b vary between $L/20$ and $L/5$, where L is the span between the columns. Figure 1 also shows the elastic distribution of shear forces along a square perimeter, where $a = b = L/10$.

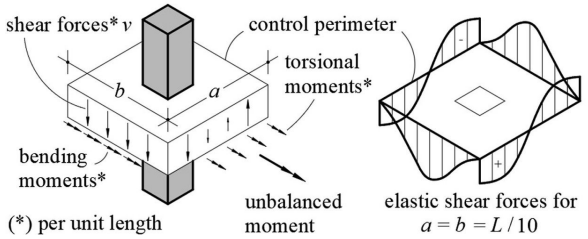

a/b	K	
	Mast	MC90
0.5	0.3	0.45
1.0	0.5	0.6
2.0	0.7	0.7
3.0	0.8	0.8

Figure 1. Unbalanced moment transfer in slab-column connections

Shear force distribution in reinforced concrete flat slabs has also been studied by nonlinear finite element analyses. Shu et al. [15] investigate internal columns without unbalanced moments in flat slabs without shear reinforcement. The shear force distributions along the control perimeters are determined by shell and solid nonlinear finite element models. The results show that reinforcement arrangement, cracking and nonlinear material behavior influence the shear force distribution. Laguta [16] uses a concrete damaged plasticity material model to describe the nonlinear behavior of the concrete and present a typical shear stress distribution at a control perimeter under combined vertical load and unbalanced moment.

Normal force and bending moment are considered separately in the MC90 design model and produce distinct plastic shear force diagrams per unit length (Figure 2). The plastic shear forces related to normal force F and bending moment M are respectively denoted by v_F and v_M.

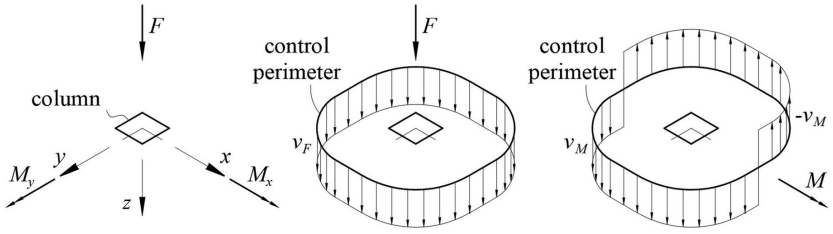

Figure 2. Coordinate system, applied forces and moments, and distributed shear forces

MC90 defines an effective normal force F_{ef}, including the effect of unbalanced moment. The plastic diagrams for normal force F and bending moment M determine the effective force F_{ef}. EC2 uses the same methodology, presented by coefficient β, such that $F_{ef} = \beta F$.

F_{ef}^{j} is here defined as the effective force that is calculated on Perimeter j. The following expressions apply:

$$v_F^j = \frac{F}{u^j} \quad ; \quad v_F^{*j} = \frac{F}{u^{*j}} \quad ; \quad v_M^j = \frac{M}{W_p^j} \tag{1}$$

where W_p^j is the plastic modulus and u^j is the developed length of Perimeter j. Reduced lengths u^{*j} are defined for edge and corner columns. Reduced lengths u^{*j} correspond to developed lengths u^j in internal columns.

The combined shear force per unit length v_{MF}^j is expressed by

$$v_{MF}^j = v_F^{*j} + v_M^j \tag{2}$$

The effective force F_{ef}^j on Perimeter j is given by

$$F_{ef}^j = \frac{v_{MF}^j}{v_F^j} F \tag{3}$$

4 PLASTIC MODULUS FOR ASYMMETRICAL BENDING

A numerical procedure is used to determine the plastic shear diagram and the plastic flexural modulus of an arbitrary perimeter, which is subjected to a bending moment M about an oblique axis.

M_x and M_y are the vector components of bending moment M about the $x-$ and $y-$axes, respectively (Figure 3).

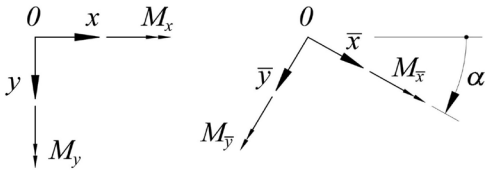

Figure 3. Rotated coordinate system associated with the principal moments

4.1 Moments in the principal coordinate system

Figure 3 presents the principal coordinate system $\bar{x}\bar{y}$. The system is rotated from the xy coordinate system by an angle α, which is defined by

$$cos\,\alpha = \frac{M_x}{\sqrt{M_x^2+M_y^2}} \quad ; \quad sin\,\alpha = \frac{M_y}{\sqrt{M_x^2+M_y^2}} \tag{4}$$

Considering $\bar{x} = x\,cos\,\alpha + y\,sin\,\alpha$ and $\bar{y} = -x\,sin\,\alpha + y\,cos\,\alpha$, the equilibrium conditions of the shear forces per unit length v along the perimeter U yield

$$M_{\bar{x}} = \int_U v\bar{y}ds = \int_U v(-x\,sin\,\alpha + y\,cos\,\alpha)ds = M_x\,cos\,\alpha + M_y\,sin\,\alpha = \sqrt{M_x^2 + M_y^2} \tag{5}$$

$$M_{\bar{y}} = \int_U -v\bar{x}ds = \int_U -v(x\,cos\,\alpha + y\,sin\,\alpha)ds = -M_x\,sin\,\alpha + M_y\,cos\,\alpha = 0 \tag{6}$$

where $M_{\bar{x}}$ and $M_{\bar{y}}$ are the moments about the $\bar{x}-$ and $\bar{y}-$axes (Figure 3).

4.2 Distribution of shear forces per unit length

Shear forces $v = -v_M$ and $v = +v_M$ (Figure 2) are considered uniformly distributed along perimeter lengths U^- and U^+, respectively. The equilibrium conditions in the $z-$direction and about the $x-$ and $y-$axes lead to the following equations:

$$\int_{U^-}(-v_M)ds + \int_{U^+}(+v_M)ds = 0 \tag{7}$$

$$M_{\bar{x}} = \int_{U^-}(-v_M)\bar{y}ds + \int_{U^+}(+v_M)\bar{y}ds \tag{8}$$

$$M_{\bar{y}} = -\int_{U^-}(-v_M)\bar{x}ds - \int_{U^+}(+v_M)\bar{x}ds \tag{9}$$

Collecting like terms in Equations 7 to 9 yields

$$\int_{U^-}(-1)ds + \int_{U^+}(+1)ds = 0 \tag{10}$$

$$W_{p\bar{x}} = \int_{U^-}(-1)\bar{y}ds + \int_{U^+}(+1)\bar{y}ds \tag{11}$$

$$W_{p\bar{y}} = -\int_{U^-}(-1)\bar{x}ds - \int_{U^+}(+1)\bar{x}ds \tag{12}$$

where the plastic flexural moduli $W_{p\bar{x}}$ and $W_{p\bar{y}}$ are

$$W_{p\bar{x}} = \frac{M_{\bar{x}}}{v_M} \quad ; \quad W_{p\bar{y}} = \frac{M_{\bar{y}}}{v_M} \tag{13}$$

A numerical algorithm establishes perimeter lengths U^- and U^+.

4.3 Discretization and parametrization of the control perimeter

The perimeter is divided into linear and arc segments for the application of the numerical procedure.

The developed length of the control perimeter is defined as u. The numerical procedure demands that all segments have lengths less than the semi-perimeter $u/2$. This condition is satisfied by the division into segments shown in Figure 4.

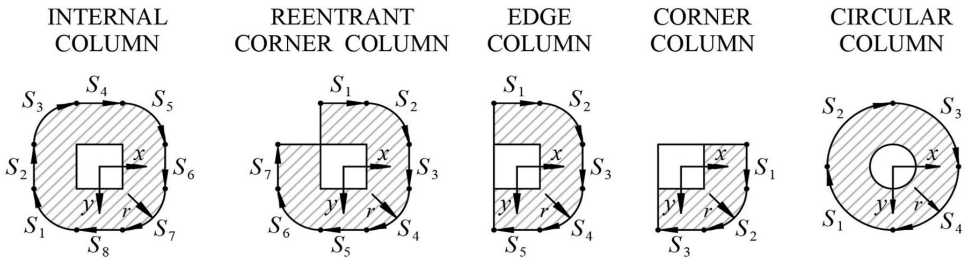

Figure 4. Discretization of control perimeters into segments S_i

The points that divide the segments are numbered from 1 to N. The control perimeter is parameterized according to the developed length s, where $s_1 = 0$ at start point 1 and $s_N = u$ at endpoint N (Figure 5).

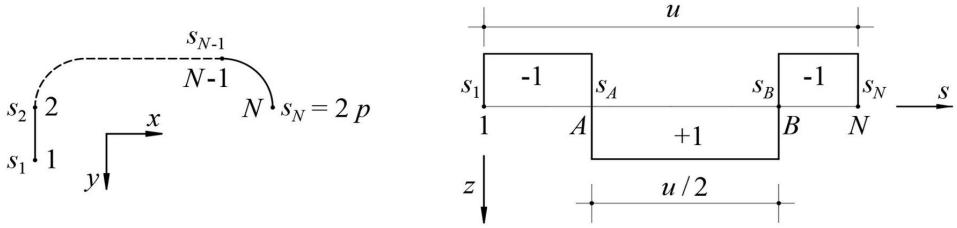

Figure 5. Parameter s and unit shear force distribution along the control perimeter

This parameterization is valid for open and closed perimeters. Points 1 and N are distinct for open perimeters but coincident for closed perimeters.

Figure 5 also presents a flat diagram of unit shear forces per unit length. The longitudinal axis indicates parameter s, which is the developed length from the origin ($s_1 = 0$). The unit shear forces change signs at points A and B. The perimeter length of positive shear forces U^+ is defined between points A and B. The perimeter length of negative shear forces U^- is defined in intervals $1 - A$ and $B - N$.

Equation 10 shows that the developed lengths of the perimeter lengths U^- and U^+ are both equal to the semi-perimeter $u/2$.

4.4 Plastic flexural modulus

The parameters s of points A and B are defined as s_A and s_B, respectively. Equation 10 is automatically respected by adopting the following

$$s_B = s_A + \frac{u}{2} \tag{14}$$

A parameter s_A yields s_B by Equation 14. Perimeter lengths U^- and U^+ are defined in Figure 5. The plastic flexural moduli $W_{p\bar{x}}(s_A)$ and $W_{p\bar{y}}(s_A)$are determined by Equations 11 and 12, respectively.

The algorithm searches for a parameter s_A^* that yields $W_{p\bar{y}}(s_A^*) \simeq 0$. The solution s_A^* yields a unit diagram proportional to the shear force diagram that satisfies Equations 5 and 6.

The plastic flexural modulus W_p and the shear force per unit length v_M are given by

$$W_p = \left|W_{p\bar{x}}(s_A^*)\right| \tag{15}$$

$$v_M = \frac{M_{\bar{x}}}{W_p} = \frac{\sqrt{M_x^2 + M_y^2}}{W_p} \tag{16}$$

where v_M is always positive.

If $\bar{y}$ coordinates are always negative in U^- and positive in U^+, or always positive in U^- and negative in U^+, Equations 11 and 15 yield

$$W_p = \int_U |\bar{y}| ds \tag{17}$$

Equation 17 cannot be used in the general case, but it is valid for symmetrical perimeters about the $\bar{x}-$ axis. It is applicable in specific cases, such as edge columns subjected to moments $M_{\bar{x}} = M_x$ (Figure 4).

4.5 Partial integration of a same-sign length of a segment

Changes in the sign of unit shear forces can occur in linear and arc segments. Equations 11 and 12 yield the plastic flexural moduli $W_{p\bar{x}}$ and $W_{p\bar{y}}$ by integrating lengths with shear forces of the same sign.

A segment's start and end points are defined as I and J, respectively (Figure 6). Points P and Q determine a length with positive shear forces.

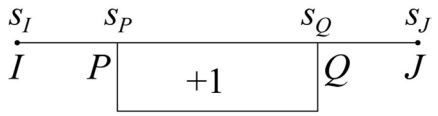

Figure 6. Partial integration between points P and Q

The variables associated with points P, Q, I, and J that are known are the parameters s_I, s_J, s_P, and s_Q and the coordinates $\bar{x}_I$, $\bar{y}_I$, $\bar{x}_J$, and $\bar{y}_J$. The dimensionless factors ζ_{GI} and ζ_{GJ} of a generic point G on the segment are defined by

$$\zeta_{GI} = \frac{(s_J - s_G)}{(s_J - s_I)} \quad ; \quad \zeta_{GJ} = \frac{(s_G - s_I)}{(s_J - s_I)} \tag{18}$$

In the case of linear segments, H is defined as the barycenter of PQ. The parameter s_H and coordinates $\bar{x}_H$ and $\bar{y}_H$ are equal to

$$s_H = \frac{(s_P + s_Q)}{2} \tag{19}$$

$$\bar{x}_H = \zeta_{HI}\bar{x}_I + \zeta_{HJ}\bar{x}_J \quad ; \quad \bar{y}_H = \zeta_{HI}\bar{y}_I + \zeta_{HJ}\bar{y}_J \tag{20}$$

where $W_{p\bar{x}}^{PQ}$ and $W_{p\bar{y}}^{PQ}$ are the contributions of PQ to the plastic moduli $W_{p\bar{x}}$ and $W_{p\bar{y}}$. In linear segments, they are expressed by

$$W_{p\bar{x}}^{PQ} = \Delta s \bar{y}_H \quad ; \quad W_{p\bar{y}}^{PQ} = -\Delta s \bar{x}_H \tag{21}$$

$$\Delta s = s_Q - s_P \tag{22}$$

where Δs is the length between P and Q.

In arc segments, the following variables are also considered: angles α_I and α_J at points I and J, coordinates x_C and y_C of the center, and radius r. Angles α_P and α_Q are interpolated by

$$\alpha_P = \zeta_{PI}\alpha_I + \zeta_{PJ}\alpha_J \quad ; \quad \alpha_Q = \zeta_{QI}\alpha_I + \zeta_{QJ}\alpha_J \tag{23}$$

The following expressions yield the contributions of PQ to the plastic moduli $W_{p\bar{x}}$ and $W_{p\bar{y}}$ in arc segments:

$$W_{p\bar{x}}^{PQ} = \int_{\alpha_P}^{\alpha_Q} 1\bar{y} ds = \int_{\alpha_P}^{\alpha_Q} 1(\bar{y}_C + r\,sin\,\alpha) r d\alpha = \Delta s \bar{y}_C + r^2\left(cos\,\alpha_Q - cos\,\alpha_P\right)$$

$$W_{p\bar{y}}^{PQ} = -\int_{\alpha_P}^{\alpha_Q} 1\bar{x} ds = -\int_{\alpha_P}^{\alpha_Q} 1(\bar{x}_C + r\,cos\,\alpha) r d\alpha = -\Delta s \bar{x}_C - r^2\left(sin\,\alpha_Q - sin\,\alpha_P\right) \tag{24}$$

The developed length Δs between P and Q is

$$\Delta s = r\left(\alpha_Q - \alpha_P\right) \tag{25}$$

4.6 Full segment integration

Unit shear forces on lengths PQ (Figure 6) can be positive or negative. Figure 7 discusses the positive and negative shear forces that should be considered during the complete integration of a segment IJ.

Each segment cannot simultaneously contain points A and B, since all segments have a developed length less than the semi-perimeter $u/2$. The discretization into segments shown in Figure 4 meets this requirement.

Parameters s_A and s_B define segments S_A and S_B, which respectively contain points A and B.

Table 1 defines the coordinates s_P and s_Q of each segment S integration step, according to its location. Equations 21 and 24 are established for a positive unit shear force. The effective signs of unit shear forces will be considered as indicated in the table.

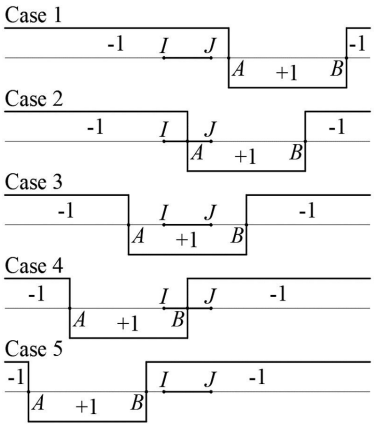

Figure 7. Unit shear force along the control perimeter

Table 1. Integration of segment IJ

Case	Condition	Segment parts	s_P	s_Q	v
1	$S < S_A$	1	s_I	s_J	-1
2	$S = S_A$	2	s_I	s_A	-1
			s_A	s_J	1
3	$S < S_B$	1	s_I	s_J	1
4	$S = S_B$	2	s_I	s_B	1
			s_B	s_J	-1
5	$S > S_B$	1	s_I	s_J	-1

5 IMPLEMENTATION AND EXAMPLES

The previous steps define an iteration that yields the plastic flexural moduli $W_{p\bar{x}}(s_A)$ and $W_{p\bar{y}}(s_A)$ as a parameter function s_A. The parameter s_A^* associated with $W_{p\bar{y}}(s_A^*) \cong 0$ gives the principal plastic modulus $W_p = \left|W_{p\bar{x}}(s_A^*)\right|$, which depends on the direction of the applied bending moment M. The solution s_A^* is searched for in the interval $0 \leq s_A < \frac{u}{2}$.

As the computational cost of the procedure is low, the solution can be investigated by sequentially examining many values in the range. This process can be optimized by dividing the original interval into m subintervals. The solution subinterval is identified by the change in the sign of $W_{p\bar{x}}$ at its endpoints, but the endpoints themselves should be previously verified as possible solutions. The solution subinterval is iteratively divided into m subintervals until the required tolerance is reached. This work uses $m = 20$.

Figure 8 shows examples of internal, reentrant corner, edge, and corner columns. All columns are subjected to unbalanced moments about an oblique $\bar{x}$ −axis, which is rotated 60 degrees from the x −axis, in the counterclockwise direction. Perimeter 1 unit shear diagrams are shown.

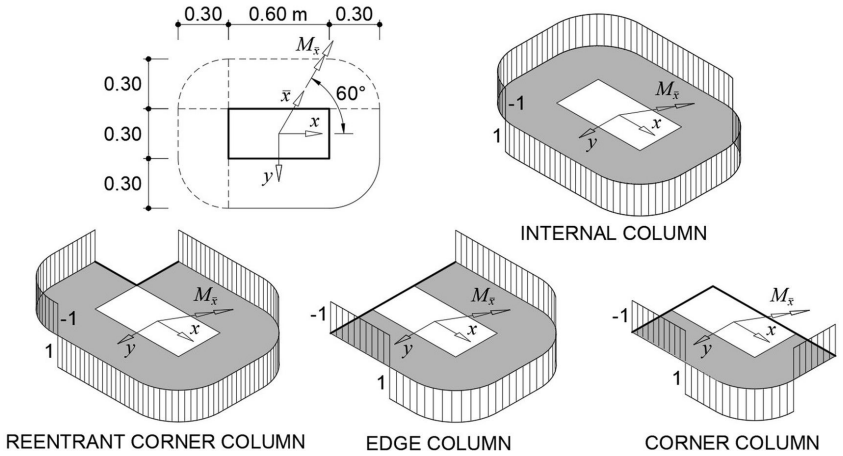

Figure 8. Examples: asymmetrical diagrams of unit shear forces

The sections of all the columns are 0.60 x 0.30 m, and all the slabs have 0.15 m effective depth.

The signs of the shear forces change in the arc and linear segments. The shear force diagrams depend on the direction of the acting bending moment and do not show symmetry.

6 COMPARISON WITH EXPERIMENTS IN THE LITERATURE

Experimental results in the literature are analyzed using MC90, EC2, and NBR6118 together with the proposed procedure.

Asymmetrical bending results can be compared with values usually accepted by these codes as the dataset also includes tests that yield symmetrical diagrams in bending.

The formulas from the codes are used with $\gamma_f = \gamma_c = \gamma_s = 1$, where γ_f is the partial factor for actions. Parameters γ_c and γ_s are the partial factors for concrete and reinforcing steel, respectively.

Shear reinforcement arrangements are always distributed uniformly in the literature tests discussed in this work. Perimeter n may be discontinuous since perimeter lengths with distances greater than d to the nearest transverse reinforcement will not be considered. For uniformly distributed shear reinforcement, the effective shear force $v_{MF,ef}$ is estimated by the following equation:

$$v_{MF,ef} = v_{MF}\frac{s_{avg}}{s_{max}} \geq v_{MF} \tag{26}$$

The combined shear force v_{MF} for continuous perimeters is determined according to each code. The average spacing between transverse bars in the outer reinforcement contour is s_{avg}. The maximum spacing $s_{max}$is defined as $2d$.

Although the procedures in EC2 and NBR6118 are based on MC90, the differences between them significantly affect the results. The following code criteria are discussed in this work:

a. Size effect (ξ)

In MC90, EC2, and NBR6118, design shear stress τ_{Rd} depends on the size effect parameter $\xi = 1 + \sqrt{\frac{0.2\text{m}}{d}}$. EC2 also assumes $\xi \leq 2$.

b. Reinforcement ratio for longitudinal reinforcement (ρ)

Design shear stress τ_{Rd} is also a function of the longitudinal reinforcement ratio $\rho = \sqrt{\rho_x \rho_y}$ in MC90, EC2, and NBR6118. Parameters ρ_x and ρ_y are the ratios in the $x-$ and y −directions, respectively. EC2 also assumes $\rho \leq 0.02$.

c. Effective design yield stress of shear reinforcement ($f_{ywd,ef}$)

All the codes limit the effective design yield stress of shear reinforcement $f_{ywd,ef}$. MC90 adopts $f_{ywd,ef} \leq 300$MPa. In EC2, the maximum value depends on the effective depth d of the slab. NBR6118 defines different limits for connectors and stirrups depending on total depth h. In this work, the NBR6118 formulation is adapted for effective depth $d = h - 0.03$m.

d. Distance between Perimeter n and the outer transverse reinforcement contour (kd)

MC90 and NBR6118 establish the distance $kd = 2d$ between Perimeter n and the outer transverse reinforcement contour. EC2 assumes $kd = 1.5d$.

e. Edge and corner column moments with internal eccentricity (M^*)

MC90 and EC2 do not consider moments with internal eccentricity in edge and corner columns. NBR6118 partially includes internal moments that are larger than M^*, which are the moments that can be resisted by eccentricities between columns and reduced control perimeters.

f. Perimeter 0 length on edge and corner columns (u^{0*})

In edge and corner column connections, MC90 and EC2 assume a reduced length for Perimeter 0, which is here denoted as u^{0*}. NBR6118 does not assume a reduced length for Perimeter 0.

g. Effective normal force due to unbalanced moments (F_{ef})

F_{ef}^{j} is defined as the effective normal force that is calculated on a control Perimeter j. MC90 uses F_{ef}^{1} and F_{ef}^{n} on Perimeters 1 and n, respectively, and reuses F_{ef}^{1} on Perimeter 0. EC2 only calculates F_{ef}^{1}, which is used as the effective normal force on all perimeters. Effective forces are not discussed in NBR6118.

h. Concrete strength reduction factor in diagonal compression (α_θ)

The concrete stress in diagonal compression is limited to $\alpha_\theta \alpha_V f_{cd}$ at Perimeter 0, where f_{cd} is the concrete design strength and $\alpha_V = \left(1 - \frac{f_{ck}}{250\text{MPa}}\right)$. The reduction factor α_θ is given as 0.30, 0.24, and 0.27 in MC90, EC2, and NBR6118, respectively.

Ten combinations (C1 to C10) of eight criteria from the codes are presented in Table 2. Combinations C1 to C3 correspond to MC90, EC2, and NBR6118, respectively. C4 to C10 investigate the response of different criteria *a* to *h* in EC2 and NBR6118.

Table 2. Combinations of criteria from Model Code 90, Eurocode 2, and NBR 6118

Combinations of criteria from codes	Criteria from the codes								$\psi \geq 0.95$	ψ_{mean}	ψ_{min}
	a	b	c	d	e	f	g	h			
	ξ	ρ	$f_{ywd,ef}$	kd	M^*	u^{0*}	F_{ef}	α_θ			
C1	MC90	MC90	MC90	MC90	MC90	MC90	MC90	MC90	64%	1.06	0.12
C2	EC2	EC2	EC2	EC2	EC2	EC2	EC2	EC2	94%	1.29	0.18
C3	NBR 6118	NBR 6118	NBR 6118	NBR 6118	NBR 6118	NBR 6118	NBR 6118	NBR 6118	67%	1.14	0.71
C4	EC2	EC2	EC2	EC2	NBR 6118	EC2	EC2	EC2	99%	1.42	0.92
C5	EC2	EC2	NBR 6118	EC2	NBR 6118	EC2	EC2	EC2	99%	1.42	0.92
C6	NBR 6118	NBR 6118	NBR 6118	EC2	NBR 6118	EC2	EC2	EC2	84%	1.20	0.71
C7	EC2	EC2	NBR 6118	NBR 6118	NBR 6118	EC2	EC2	EC2	97%	1.39	0.89
C8	EC2	EC2	NBR 6118	EC2	NBR 6118	NBR 6118	EC2	EC2	99%	1.42	0.92
C9	EC2	EC2	NBR 6118	EC2	NBR 6118	EC2	MC90	EC2	98%	1.40	0.89
C10	EC2	EC2	NBR 6118	EC2	NBR 6118	EC2	EC2	NBR 6118	98%	1.41	0.82
C5 - Asym.	EC2	EC2	NBR 6118	EC2	NBR 6118	EC2	EC2	EC2	100%	1.66	1.06

MC90 = Model Code 90; EC2 = Eurocode 2; NBR = Norma Brasileira (Brazilian Code); ψ = ratio between the experimental and estimated capacities; ψ_{mean} = mean value of ψ ; ψ_{min} = minimum value of ψ

Ninety-four experiments of slab-column connections subjected to punching shear were compiled from the literature and their experimental capacity was compared with the theoretical capacity given by the combinations in Table 2. The dataset contains internal, reentrant corner, edge, and corner columns subjected to normal forces, with and without unbalanced moments. The tests include slabs without shear reinforcement. Transverse reinforcement is provided by shear studs.

Table 3. C5 results for experiments in Stamenkovic [17] and Stamenkovic and Chapman [18].

Exp.	Case	d	c_x	c_y	ρ	f_{ck}	F	M_x	M_y	F^1_{ef}	A^{ϕ}_{sw}	n_p	n_r	s_0	s_r	f_{ywk}	$f_{ywk,ef}$	s_{avg}	s_{max}	Crit. per.	ψ
		(mm)	(mm)	(mm)	(%)	(MPa)	(kN)	(kNm)	(kNm)	(kN)	(cm²)			(mm)	(mm)	(MPa)	(MPa)	(mm)	(mm)		
V_I_1	INTERNAL	56	127	127	1.17	40.14	119.7	-	-	119.7	-	-	-	-	-	-	-	-	-	1	1.36
V_I1_1	INTERNAL	56	127	127	1.17	38.68	104.5	-	-	104.5	-	-	-	-	-	-	-	-	-	1	1.20
V_I2_1	INTERNAL	56	127	127	2.34	56.26	129.9	-	-	129.9	-	-	-	-	-	-	-	-	-	1	1.10
V_I_2	INTERNAL	56	127	127	1.17	27.54	117.4	-	-	117.4	-	-	-	-	-	-	-	-	-	1	1.51
V_Ir_1	INTERNAL	56	152	76	1.17	26.72	108.5	-	-	108.5	-	-	-	-	-	-	-	-	-	1	1.48
V_E_1	EDGE	56	127	127	1.17	30.47	74.7	-	-	74.7	-	-	-	-	-	-	-	-	-	1	1.86
V_C_1	CORNER	56	127	127	1.17	34.23	27.1	-	-	27.1	-	-	-	-	-	-	-	-	-	1	1.30
C_I_1	INTERNAL	56	127	127	1.17	38.27	84.5	-	-7.3	120.6	-	-	-	-	-	-	-	-	-	1	1.39
C_I_2	INTERNAL	56	127	127	1.17	31.53	62.3	-	-10.5	114.0	-	-	-	-	-	-	-	-	-	1	1.41
C_I_3	INTERNAL	56	127	127	1.17	27.13	33.8	-	-13.6	101.1	-	-	-	-	-	-	-	-	-	1	1.31
C_I_4	INTERNAL	56	127	127	1.17	26.67	20.9	-	-16.7	103.1	-	-	-	-	-	-	-	-	-	1	1.34
C_Ir_1	INTERNAL	56	152	76	1.17	24.03	85.7	-	-7.3	127.0	-	-	-	-	-	-	-	-	-	1	1.79
C_Ir_2	INTERNAL	56	152	76	1.17	31.06	67.3	-	-10.9	128.6	-	-	-	-	-	-	-	-	-	1	1.66
C_Ir_3	INTERNAL	56	152	76	1.17	30.36	39.9	-	-15.7	128.6	-	-	-	-	-	-	-	-	-	1	1.68
C_Ir_4	INTERNAL	56	152	76	1.17	28.25	21.6	-	-16.8	116.5	-	-	-	-	-	-	-	-	-	1	1.56
Ct_E_1	EDGE	56	127	127	1.17	29.60	45.8	4.9	-	59.6	-	-	-	-	-	-	-	-	-	1	1.50
Ct_E_2	EDGE	56	127	127	1.17	30.18	34.9	5.7	-	51.1	-	-	-	-	-	-	-	-	-	1	1.28
Ct_E_3	EDGE	56	127	127	1.17	29.65	23.5	9.4	-	50.1	-	-	-	-	-	-	-	-	-	1	1.26
Ct_E_4	EDGE	56	127	127	1.17	31.06	12.9	10.1	-	41.6	-	-	-	-	-	-	-	-	-	1	1.03
Cn_E_1	EDGE	56	127	127	1.17	32.70	73.2	-	-5.6	73.2	-	-	-	-	-	-	-	-	-	1	1.78
Cn_E_2	EDGE	56	127	127	1.17	27.54	54.7	-	-9.2	76.4	-	-	-	-	-	-	-	-	-	1	1.97
Cn_E_3	EDGE	56	127	127	1.17	28.89	24.9	-	-10.1	85.5	-	-	-	-	-	-	-	-	-	1	2.17
Cn_E_4	EDGE	56	127	127	1.17	29.19	10.9	-	-8.8	75.7	-	-	-	-	-	-	-	-	-	1	1.91
C_C_1	CORNER	56	127	127	1.17	32.35	24.9	-	-6.2	56.7	-	-	-	-	-	-	-	-	-	1	2.78
C_C_2	CORNER	56	127	127	1.17	30.06	15.9	-	-6.4	60.0	-	-	-	-	-	-	-	-	-	1	3.01
C_C_3	CORNER	56	127	127	1.17	27.43	8.0	-	-6.2	59.6	-	-	-	-	-	-	-	-	-	1	3.08
C_C_4	CORNER	56	127	127	1.17	32.53	3.6	-	-5.6	55.1	-	-	-	-	-	-	-	-	-	1	2.69

Table 4. C5 results for experiments in Ferreira [19] and Ferreira et al. [20].

Exp.	Case	d	c_x	c_y	ρ	f_{ck}	F	M_x	M_y	F^1_{ef}	A^{ϕ}_{sw}	n_p	n_r	s_0	s_r	f_{ywk}	$f_{ywk,ef}$	s_{avg}	s_{max}	Crit. per.	ψ
		(mm)	(mm)	(mm)	(%)	(MPa)	(kN)	(kNm)	(kNm)	(kN)	(cm²)			(mm)	(mm)	(MPa)	(MPa)	(mm)	(mm)		
LC01	CIRCULAR	143	270	270	1.5	48.00	858.4	-	-	858.4	0.79	6	10	70	100	573.0	363.0	436	286	*n*	1.06
LC02	CIRCULAR	140	360	360	1.55	47.00	955.7	-	-	955.7	0.79	6	10	70	100	573.0	360.0	465	280	*n*	1.25
LC03	CIRCULAR	142	450	450	1.41	49.00	1076.8	-	-	1076.8	0.79	6	10	70	100	573.0	362.0	493	284	*n*	1.41
LC05	CIRCULAR	140	360	360	2.05	50.00	1117.5	-	-	1117.5	0.79	6	10	70	100	573.0	360.0	465	280	*n*	1.32
LC06	CIRCULAR	143	360	360	1.45	49.00	1077.9	-	-	1077.9	0.79	6	10	70	100	573.0	363.0	465	286	*n*	1.36
LC07	CIRCULAR	144	360	360	1.6	49.00	1110.4	-	-	1110.4	0.79	7	10	55	80	573.0	364.0	442	288	*n*	1.31
LC08	CIRCULAR	144	360	360	1.62	48.00	1058.9	-	-	1058.9	0.79	6	12	70	100	573.0	364.0	387	288	*n*	1.06

Table 5. C5 results for experiments in Ferreira [19] and Ferreira et al. [21].

Exp.	Case	d	c_x	c_y	ρ	f_{ck}	F	M_x	M_y	F^1_{ef}	A^{ϕ}_{sw}	n_p	n_r	s_0	s_r	f_{ywk}	$f_{ywk,ef}$	s_{avg}	s_{max}	Crit. per.	ψ
		(mm)	(mm)	(mm)	(%)	(MPa)	(kN)	(kNm)	(kNm)	(kN)	(cm²)			(mm)	(mm)	(MPa)	(MPa)	(mm)	(mm)		
LS01	INTERNAL	145	300	300	1.54	48.00	1021.5	-	-	1021.5	0.79	2	12	70	100	573.0	364.0	177	290	*n*	1.38
LS02	INTERNAL	143	300	300	1.46	49.00	1127.5	-	-	1127.5	0.79	4	12	70	100	573.0	363.0	278	286	*n*	1.14
LS03	INTERNAL	145	300	300	1.54	50.00	698.5	-	-189.0	1071.5	0.79	2	12	70	100	573.0	364.0	177	290	*n*	1.43
LS04	INTERNAL	143	300	300	1.46	49.00	721.7	-	-190.0	1099.9	0.79	4	12	70	100	573.0	363.0	278	286	*n*	1.12
LS05	INTERNAL	143	300	300	1.58	50.00	779.0	-	-	779.0	-	-	-	-	-	-	-	-	-	1	1.18
LS06	INTERNAL	144	300	300	1.56	50.00	528.3	-	-140.7	807.2	-	-	-	-	-	-	-	-	-	1	1.21
LS07	INTERNAL	143	300	300	1.7	49.00	1196.8	-	-	1196.8	1.23	4	12	70	100	530.0	363.0	280	286	*n*	1.15
LS08	INTERNAL	144	300	300	1.68	48.00	934.1	-	-190.9	1312.5	1.23	4	12	70	100	530.0	364.0	280	288	*n*	1.27

Table 6. C5 results for experiments in Feliciano [22].

Exp.	Case	d	c_x	c_y	ρ	f_{ck}	F	M_x	M_y	F^1_{ef}	A^{ϕ}_{sw}	n_p	n_r	s_0	s_r	f_{ywk}	$f_{ywk,ef}$	s_{avg}	s_{max}	Crit. per.	ψ
		(mm)	(mm)	(mm)	(%)	(MPa)	(kN)	(kNm)	(kNm)	(kN)	(cm²)			(mm)	(mm)	(MPa)	(MPa)	(mm)	(mm)		
L1	EDGE	152	300	300	0.75	45.10	293.0	-	-87.8	293.0	-	-	-	-	-	-	-	-	-	1	1.06
L2	EDGE	152	300	300	0.75	45.10	300.0	-	-	300.0	-	-	-	-	-	-	-	-	-	1	1.09
L3	EDGE	152	300	300	0.75	45.10	242.0	-	72.5	493.7	-	-	-	-	-	-	-	-	-	1	1.79
L4	EDGE	152	300	300	0.75	45.10	198.0	-	79.0	472.1	-	-	-	-	-	-	-	-	-	1	1.72

Table 7. C5 results for experiments in Barbosa [23].

Exp.	Case	d	c_x	c_y	ρ	f_{ck}	F	M_x	M_y	F_{ef}^1	A_{sw}^{ϕ}	n_p	n_r	s_0	s_r	f_{ywk}	$f_{ywk,ef}$	s_{avg}	s_{max}	Crit. per.	ψ
		(mm)	(mm)	(mm)	(%)	(MPa)	(kN)	(kNm)	(kNm)	(kN)	(cm²)			(mm)	(mm)	(MPa)	(MPa)	(mm)	(mm)		
L01	REENTRANT	144	300	300	1.4	57.90	300.0	111.4	-111.4	624.7	-	-	-	-	-	-	-	-	-	1	1.23
L02	REENTRANT	144	300	300	1.4	57.90	488.0	120.8	-120.8	840.2	0.5	3	10	70	100	587.0	364.0	231	288	*n*	1.25
L03	REENTRANT	144	300	300	1.4	57.90	550.0	136.1	-136.1	946.9	0.78	4	10	70	100	562.0	364.0	282	288	*n*	1.22
L04	REENTRANT	144	300	300	1.4	57.90	347.0	85.9	-85.9	597.4	-	-	-	-	-	-	-	-	-	1	1.18

Table 8. C5 results for experiments in Oliveira [24].

Exp.	Case	d	c_x	c_y	ρ	f_{ck}	F	M_x	M_y	F_{ef}^1	A_{sw}^{ϕ}	n_p	n_r	s_0	s_r	f_{ywk}	$f_{ywk,ef}$	s_{avg}	s_{max}	Crit. per.	ψ
		(mm)	(mm)	(mm)	(%)	(MPa)	(kN)	(kNm)	(kNm)	(kN)	(cm²)			(mm)	(mm)	(MPa)	(MPa)	(mm)	(mm)		
LN01	INTERNAL	143	400	200	1.58	55.10	1084.0	-	-	1084.0	0.5	3	14	70	100	573.0	363.0	201	286	*n*	1.17
LN02	INTERNAL	143	400	200	1.58	53.80	1144.0	-	-	1144.0	0.5	6	14	70	100	573.0	363.0	334	286	1	1.08
LN03	INTERNAL	143	400	200	1.58	51.20	786.0	-	-	786.0	-	-	-	-	-	-	-	-	-	1	1.18
LN04	INTERNAL	143	400	200	1.58	55.50	966.0	-	-	966.0	0.31	4	14	70	100	651.0	363.0	245	286	1	1.13
LN05	INTERNAL	142	400	200	1.6	54.80	1143.0	-	-	1143.0	1.23	5	14	70	100	602.0	362.0	290	284	*n*	0.97
LS01	INTERNAL	143	400	200	1.58	53.60	425.0	-	-114.0	673.9	-	-	-	-	-	-	-	-	-	1	0.99
LS02	INTERNAL	144	400	200	1.56	53.90	763.0	-	-218.0	1237.0	0.5	3	14	70	100	573.0	364.0	201	288	*n*	1.33
LS03	INTERNAL	142	400	200	1.6	54.40	775.0	-	-234.0	1287.9	0.5	6	14	70	100	573.0	362.0	334	284	1	1.23
LS04	INTERNAL	143	400	200	1.58	51.30	712.0	-	-183.0	1111.5	0.31	4	14	70	100	651.0	363.0	245	286	1	1.32
LS05	INTERNAL	142	400	200	1.6	51.00	926.0	-	-272.0	1522.2	1.23	5	14	70	100	602.0	362.0	290	284	*n*	1.32
LS06	INTERNAL	143	400	200	1.58	53.00	904.0	-	-252.0	1454.1	0.79	6	14	70	100	597.0	363.0	334	286	*n*	1.27
LW01	INTERNAL	141	200	400	1.62	50.20	446.0	-	-124.0	648.0	-	-	-	-	-	-	-	-	-	1	0.99
LW02	INTERNAL	143	200	400	1.58	52.20	711.0	-	-189.0	1016.0	0.5	3	14	70	100	573.0	363.0	201	286	*n*	1.11
LW03	INTERNAL	142	200	400	1.6	51.50	733.0	-	-195.0	1049.2	0.5	6	14	70	100	573.0	362.0	319	284	1	1.01
LW04	INTERNAL	142	200	400	1.6	51.50	617.0	-	-131.0	829.4	0.31	4	14	70	100	651.0	362.0	245	284	1	0.99
LW05	INTERNAL	142	200	400	1.6	50.60	815.0	-	-241.0	1205.8	1.23	5	14	70	100	602.0	362.0	290	284	*n*	1.05

Table 9. C5 results for experiments in Trautwein et al. [25].

Exp.	Case	d	c_x	c_y	ρ	f_{ck}	F	M_x	M_y	F_{ef}^1	A_{sw}^{ϕ}	n_p	n_r	s_0	s_r	f_{ywk}	$f_{ywk,ef}$	s_{avg}	s_{max}	Crit. per.	ψ
		(mm)	(mm)	(mm)	(%)	(MPa)	(kN)	(kNm)	(kNm)	(kN)	(cm²)			(mm)	(mm)	(MPa)	(MPa)	(mm)	(mm)		
L1	INTERNAL	159	200	200	1.2	36.80	1050.0	-	-	1050.0	1.25	11	16	35	60	500.0	375.0	300	318	0	1.10
L4	INTERNAL	164	200	200	1.2	43.40	1038.0	-	-	1038.0	2	11	16	35	60	500.0	379.0	300	328	0	0.92
L9	INTERNAL	154	200	200	1.3	39.40	933.0	-	-	933.0	0.8	11	16	35	60	500.0	371.0	300	308	0	0.95

Table 10. C5 results for experiments in Albuquerque et al. [26] and Albuquerque [27].

Exp.	Case	d	c_x	c_y	ρ	f_{ck}	F	M_x	M_y	F_{ef}^1	A_{sw}^{ϕ}	n_p	n_r	s_0	s_r	f_{ywk}	$f_{ywk,ef}$	s_{avg}	s_{max}	Crit. per.	ψ
		(mm)	(mm)	(mm)	(%)	(MPa)	(kN)	(kNm)	(kNm)	(kN)	(cm²)			(mm)	(mm)	(MPa)	(MPa)	(mm)	(mm)		
L01	REENTRANT	148	300	300	2.07	48.00	325.0	114.9	-114.9	655.5	-	-	-	-	-	-	-	-	-	1	1.17
L02	REENTRANT	148	300	300	2.07	48.00	513.0	127.7	-127.7	880.3	0.5	3	10	70	100	587.0	367.0	231	296	*n*	1.19
L03	REENTRANT	145	300	300	2.17	48.00	575.0	141.9	-141.9	987.3	0.78	4	10	70	100	560.0	364.0	282	290	*n*	1.19
L04	REENTRANT	147	300	300	2.1	48.00	372.0	91.8	-91.8	637.0	-	-	-	-	-	-	-	-	-	1	1.15
L05	REENTRANT	143	300	300	0.91	44.00	250.0	89.1	-89.1	510.7	-	-	-	-	-	-	-	-	-	1	1.29
L06	REENTRANT	145	300	300	0.88	44.00	282.0	68.4	-68.4	480.8	-	-	-	-	-	-	-	-	-	1	1.20
L07	REENTRANT	141	300	300	1.35	44.00	358.0	88.3	-88.3	618.3	-	-	-	-	-	-	-	-	-	1	1.40
L08	REENTRANT	146	300	300	1.27	44.00	345.0	84.7	-84.7	590.2	-	-	-	-	-	-	-	-	-	1	1.29
L09	REENTRANT	148	300	300	2.08	43.00	550.0	135.7	-135.7	940.4	0.78	5	13	60	90	528.0	367.0	250	296	*n*	1.07
L10	REENTRANT	148	300	300	2.08	43.00	500.0	176.1	-176.1	1006.5	0.78	5	10	70	90	528.0	367.0	334	296	*n*	1.28
L11	REENTRANT	147	300	300	2.11	43.00	640.0	120.8	-120.8	988.7	0.78	5	10	70	90	528.0	366.0	334	294	*n*	1.27
L12	REENTRANT	145	300	300	1.28	43.00	345.0	65.4	-65.4	535.0	-	-	-	-	-	-	-	-	-	1	1.19

Table 11. C5 results for experiments in Albuquerque [28] and Albuquerque et al. [29].

Exp.	Case	d	c_x	c_y	ρ	f_{ck}	F	M_x	M_y	F_{ef}^1	A_{sw}^{ϕ}	n_p	n_r	s_0	s_r	f_{ywk}	$f_{ywk,ef}$	s_{avg}	s_{max}	Crit.	ψ
		(mm)	(mm)	(mm)	(%)	(MPa)	(kN)	(kNm)	(kNm)	(kN)	(cm²)			(mm)	(mm)	(MPa)	(MPa)	(mm)	(mm)	per.	
L1	EDGE	147	300	300	1	46.80	308.0	-	-92.0	308.0	-	-	-	-	-	-	-	-	-	1	1.06
L2	EDGE	146	300	300	1.25	44.70	315.0	-	-	315.0	-	-	-	-	-	-	-	-	-	1	1.03
L3	EDGE	146	300	300	1.25	45.10	256.0	-	77.0	527.2	-	-	-	-	-	-	-	-	-	1	1.72
L4	EDGE	146	300	300	1.25	46.00	210.0	-	84.0	505.8	-	-	-	-	-	-	-	-	-	1	1.64
L5	EDGE	146	300	300	1.25	51.40	374.0	-	37.0	504.3	-	-	-	-	-	-	-	-	-	1	1.58
L6	EDGE	146	300	300	1.25	52.10	330.0	-	66.0	562.4	-	-	-	-	-	-	-	-	-	1	1.75
L7	EDGE	146	300	300	1.52	50.00	288.0	-	115.0	693.0	-	-	-	-	-	-	-	-	-	1	2.05
L8	EDGE	146	300	300	1.4	50.50	320.0	-	128.0	770.8	-	-	-	-	-	-	-	-	-	1	2.34
L9	EDGE	146	300	300	1.25	57.60	489.0	-	-	489.0	0.5	4	7	70	100	580.0	365.0	287	292	*n*	0.96
L10	EDGE	146	300	300	1.52	59.30	445.0	-	89.0	758.4	0.5	4	7	70	100	580.0	365.0	287	292	*n*	1.39
L11	EDGE	146	300	300	1.52	43.10	304.0	-	110.0	691.4	-	-	-	-	-	-	-	-	-	1	2.15
L12	EDGE	146	300	300	1.52	43.60	347.0	-	55.0	540.7	-	-	-	-	-	-	-	-	-	1	1.68
L13	EDGE	146	300	300	1.52	44.10	357.0	-	125.0	797.2	-	-	-	-	-	-	-	-	-	1	2.46

Tables 3 to 11 present the results of all the experiments retrieved from the literature for the C5 combination. The sides of the columns are c_x and c_y, respectively, in the $x-$ and $y-$directions. Characteristic strength f_{ck} is substituted in the code equations by the as-tested compressive strength of concrete. Transverse reinforcement is arranged in n_p contours and n_r rails. A_{sw}^{ϕ} is one bar area. The distance from the first reinforcement contour to the column and the distance between the reinforcement contours are denoted as s_0 and s_r, respectively.

The slab capacity is verified at Perimeters 0, 1, and n. The critical control perimeters are shown in Tables 3 to 11. The prediction ratio ψ is the ratio between the experimental and estimated capacities, considering $\gamma_f = \gamma_c = \gamma_s = 1$.

A brittle failure of a slab-column connection can cause the progressive collapse of the structure. Table 2 shows the percentages of experiments with $\psi \geq 0.95$ in each combination, which indicates the reliability of the combination. Table 2 also presents the mean and the minimum ψ ratios of each combination, which are denoted as ψ_{mean} and ψ_{min}, respectively.

C1, C2, and C3 correspond to MC90, EC2, and NBR6118, respectively. Among them, C2 (EC2) gives the highest number of predictions with $\psi \geq 0.95$ (94%). C2 yields inadequate predictions in some cases. The minimum C2 prediction ratio ($\psi_{min} = 0.18$) is associated with the corner column connection C_C_4 in Stamenkovic and Chapman [18], which is subjected to unbalanced moment. The normal force is relatively small.

Combination C4 corresponds to EC2 with the moment approach proposed by NBR6118 for edge and corner columns (criteria *e*). Combinations C5 to C10 discuss the effect of replacing other criteria in C4.

Combinations C4, C5, and C8 yield $\psi \geq 0.95$ for 99% of the dataset. The average and minimum prediction ratios are $\psi_{mean} = 1.42$ and $\psi_{min} = 0.92$, respectively. The minimum prediction ratio is associated with the specimen L4 in Trautwein et al. [25], which fails at Perimeter 0 by diagonal compression in concrete. The moment criterion proposed by NBR6118 yields good capacity predictions for edge and corner column connections with internal eccentricities.

Combinations C4 and C5 show that the criteria proposed by NBR6118 and EC2 for effective yield stress $f_{ywd,ef}$ provide similar results.

Combination C8 investigates the criterion *f* from NBR 6118, by which the effective length of Perimeter 0 is not reduced in edge and corner columns. New studies are needed as the current dataset does not contain failures due to diagonal compressive stresses in edge and corner column connections.

Combinations C6, C7, and C10 show that criteria *a* (ξ), *b* (ρ), *d* (kd), and *h* (α_θ) from NBR6118 do not contribute to C5 predictions.

Combinations C5 and C9 apply the effective forces F_{ef}^1 and F_{ef}^n at Perimeter n, as recommended by EC2 and MC90, respectively. They both yield similar predictions, but this conclusion is limited to the uniformly distributed reinforcement arrangements of the dataset. Non-uniform reinforcement distributions can change the effective F_{ef}^n forces. Cross arrangements of shear reinforcement demand further investigation.

The dataset contains 16 reentrant corner columns, five corner columns, and 18 edge columns yielding asymmetrical plastic shear diagrams. Row "C5-Asym." of Table 2 discusses the results of combination C5 for the asymmetrical subset. Relations $\psi_{mean} = 1.66$ and $\psi_{min} = 1.06$ are considered adequate and compatible with the results of the complete set.

7 CONCLUSIONS

A numerical procedure yields plastic diagrams of shear forces in arbitrary control perimeters subjected to asymmetrical bending. Examples of internal, reentrant corner, edge, and corner columns are subjected to unbalanced moments about an axis oblique to the principal axes. The proposed procedure is fast, robust, and accurate.

Experimental results in the literature are compared to the MC90, EC2, and NBR6118 design methods, which are applied together with the proposed procedure.

Although the recommendations in EC2 and NBR6118 are based on MC90, they contain some differences, which are discussed as they significantly affect the results.

EC2 performed better than the other two codes. A similar conclusion is reported by Ferreira et al. [21] when comparing ACI, EC2 and Model Code 2010 [7]. However, some results of EC2 were not considered satisfactory, because this code disregards the moments of corner and edge columns with internal eccentricities.

NBR6118 considers the portions of the unbalanced moments that exceed the moments that can be resisted by the eccentricities between columns and reduced control perimeters of corner and edge columns. The best performance is obtained by combining EC2 with the NBR6118 moment criterion. Ninety-nine percent of the dataset yields prediction to experimental results ratios greater than 0.95. All prediction to experimental rates are greater than 0.92.

The prediction to experimental ratios of cases with symmetrical and asymmetrical plastic diagrams are compatible.

Asymmetrical shear diagrams are found not only in edge and corner column connections but also in internal column connections. The proposed procedure considers the asymmetrical plastic diagrams that usually occur in all column connections due to biaxial bending.

Connections of edge and corner columns, critical at Perimeter 0, and plastic shear diagrams, discontinuous due to cross-arranged reinforcement, are themes for future studies.

REFERENCES

[1] Comité Européen de Normalisation, *Eurocode 2 - Design of concrete structures – Part 1-1: General rules and rules for Buildings,* Stockholm, Sweden: Comité Européen de Normalisation, 2004.

[2] Associação Brasileira de Normas Técnicas, *Design of Concrete Structures – Procedures, NBR 6118,* 2014.

[3] Comité Euro-International du Béton, *Model Code 1990 for structures.* London, England: Comité Euro-International du Béton, 1993.

[4] P. E. Regan, *Behavior of Reinforced Concrete Flat Slabs. Report 89*. London, England: CIRIA, 1981.

[5] P. E. Regan and M. W. Braestrup, *Punching Shear in Reinforced Concrete* (Bulletin d'Information, 168). London, England: Comité Euro-International du Béton, Jan., 1985.

[6] American Concrete Institute, *Building Code Requirements for Structural Concrete and Commentary*, ACI 318R-19, 2019.

[7] Fédération Internationale du Béton, *fib Model Code for Concrete Structures, Model Code 2010*. Lausanne, Switzerland: Fédération Internationale du Béton, 2012.

[8] J. di Stasio and M. P. van Buren, "Transfer of bending moment between flat plate floor and column," *ACI J. Proc.*, vol. 57, pp. 299–314, Jan 1960, http://dx.doi.org/10.14359/8022.

[9] A. Muttoni, "Punching shear strength of reinforced concrete slabs without transverse reinforcement," *ACI Struct. J.*, vol. 105, no. 4, pp. 440–450, Jul 2008, http://dx.doi.org/10.14359/19858.

[10] M. F. Ruiz and A. Muttoni, "Applications of critical shear crack theory to punching of reinforced concrete slabs with transverse reinforcement," *ACI Struct. J.*, vol. 106, no. 4, pp. 485–494, Jul. 2009, http://dx.doi.org/10.14359/56614.

[11] Fédération Internationale du Béton, *Textbook on Behaviour, Design and Performance, vol. 2: Basis of Design* (Bulletin d'Information, 2). Lausanne, Switzerland: Fédération Internationale du Béton, 1999.

[12] N. W. Hanson and J. N. Hanson, "Shear and moment transfer between concrete slabs and columns", *J. of the PCA Rsrch. and Devel. Lab.*, vol. 10, no. 1, pp. 2–16, Jan. 1968.

[13] P. E. Mast, "Stresses in flat plates near columns," *ACI J. Proc.*, vol. 67, no. 10, pp. 761–768, Oct. 1970, http://dx.doi.org/10.14359/7306.

[14] K. Girkmann, *Flaechentragwerke : Einführung in Die Elastostatik der Scheiben, Platten, Schalen und Faltwerke*, 5th ed. Wien, Austria, Springer-Verlag, 1959.

[15] J. Shu, B. Belleti, A. Muttoni, M. Scolari, and M. Plos, "Internal force distribution in RC slabs subjected to punching shear," *Eng. Struct.*, vol. 153, pp. 766–781, Dec 2017, http://dx.doi.org/10.1016/j.engstruct.2017.10.005.

[16] M. Laguta, "Effect of unbalanced moment on punching shear strength of slab- column joints", M.S. thesis, Civil and Env. Eng., Univ. Waterloo, Ontario, 2020. [Online]. Available: https://uwspace.uwaterloo.ca/handle/10012/15931?show=full

[17] A. Stamenkovic, "Local strength of flat slabs at column heads", Ph.D. thesis, Imperial Coll. of Sci. and Tec., Univ. of London, London, 1969. [Online]. Available: https://spiral.imperial.ac.uk/bitstream/10044/1/16718/2/Stamenkovic-A-1970-PhD-Thesis.pdf

[18] A. Stamenkovic and J. C. Chapman, "Local strength at column heads in flat slabs subjected to a combined vertical and horizontal loading," *Proc. Inst. Civ. Eng.*, vol. 57, pp. 205–232, Jun. 1974, http://dx.doi.org/10.1680/iicep.1974.4054.

[19] M. P. Ferreira, "Punção em lajes lisas de concreto armado com armaduras de cisalhamento e momentos desbalanceados", Ph.D. dissertation, Fac. Tecnol., Univ. Brasília, Brasília, 2010. [Online]. Available: https://repositorio.unb.br/handle/10482/8965

[20] M. P. Ferreira, G. S. S. A. Melo, P. E. Regan, and R. L. Vollum, "Punching of reinforced concrete flat slabs with double-headed shear reinforcement," *ACI Struct. J.*, vol. 111, no. 2, pp. 363–374, Jan. 2014, http://dx.doi.org/10.14359/51686535.

[21] M. P. Ferreira, M. H. Oliveira, and G. S. S. A. Melo, "Tests on the punching resistance of flat slabs with unbalanced moments," *Eng. Struct.*, vol. 196, no. July, 2019, http://dx.doi.org/10.1016/j.engstruct.2019.109311.

[22] F. M. H. Feliciano, "Punção em lajes lisas de concreto armado com pilares de borda e excentricidade externa", M.S. thesis, Fac. Tecnol., Univ. Brasília, Brasília, 2011. [Online]. Available: https://repositorio.unb.br/handle/10482/9354

[23] W. C. S. Barbosa, "Punção em lajes lisas de concreto armado com pilares de canto reentrante", M.S. thesis, Fac. Tecnol., Univ. Brasília, Brasília, 2012. [Online]. Available: https://repositorio.unb.br/handle/10482/10968

[24] M. H. Oliveira, "Punção em lajes lisas com armadura de cisalhamento submetidas a carregamento excêntrico e apoiadas sobre pilares retangulares", Ph.D. dissertation, Fac. Tecnol., Univ. Brasília, Brasília, 2013. [Online]. Available: https://repositorio.unb.br/handle/10482/13624.

[25] L. M. Trautwein, R. B. Gomes and G. S. S. A. Melo, "Puncionamento em lajes planas de concreto armado com armadura de cisalhamento interna", vol. 7, no. 1, pp. 38-49, Nov., 2013, http://dx.doi.org/10.5216/reec.v7i1.24333.

[26] E. J. P. Albuquerque, G. S. S. A. Melo, A. M. P. Ramos and V. J. G. Lúcio, "Estudo teórico-experimental da resistência ao punçoamento de lajes fungiformes de betão armado com pilar de canto reentrante sem armadura de punçoamento", In 5ª JPEE, Lisboa, Portugal, 2014. http://dx.doi.org/10.13140/2.1.1473.1849.

[27] E. J. P. Albuquerque, "Punção em lajes lisas com armadura de cisalhamento e pilar de canto reentrante", Ph.D. dissertation, Fac. Tecnol., Univ. Brasília, Brasília, 2015. [Online]. Available: https://repositorio.unb.br/handle/10482/18905

[28] N. G. B. Albuquerque, "Comportamento das ligações de lajes lisas de concreto armado com pilares de borda sujeitas a excentricidades interna e externas", Ph.D. dissertation, Fac. Tecnol., Univ. Brasília, Brasília, 2014. [Online]. Available: https://repositorio.unb.br/handle/10482/17442

[29] N. G. B. Albuquerque, G. S. S. A. Melo, and R. L. Vollum, "Punching shear strength of flat slab-edge column connections with outward eccentricity of loading," *ACI Struct. J.*, vol. 113, no. 5, pp. 1117–1129, Sep. 2016, http://dx.doi.org/10.14359/51689156.

Author contributions: MNS: literature review, numerical tests, validation, writing, proofreading; MSPLP: conceptualization, literature review, methodology, writing, proofreading, supervision; MS: conceptualization, literature review, methodology, formal analysis, computer programming, validation, writing, proofreading, supervision.

Editors: Leandro Trautwein, Mauro Real, Mario Pimentel.